An Efficient Indirect RBFN-Based Method for Numerical Solution of PDEs

Nam Mai-Duy [a,*] and Thanh Tran-Cong [b]

[a] School of Aerospace, Mechanical and Mechatronic Engineering,

The University of Sydney, NSW 2006, Australia

[b] Faculty of Engineering and Surveying,

The University of Southern Queensland, Toowoomba, QLD 4350, Australia

Submitted to *Numerical Methods for Partial Differential Equations*

23 December 2003, revised 8 November 2004

*Corresponding author: Tel.: +61 2 9351 7151, Fax: +61 2 9351 7060, E-mail: nam.maiduy@aeromech.usyd.edu.au

Abstract This paper presents an efficient indirect radial basis function network (RBFN) method for numerical solution of partial differential equations (PDEs). Previous findings showed that the RBFN method based on an integration process (IRBFN) is superior to the one based on a differentiation process (DRBFN) in terms of solution accuracy and convergence rate [1]. However, when the problem dimensionality N is greater than 1, the size of the system of equations obtained in the former is about N times as big as that in the latter. In this paper, prior conversions of the multiple spaces of network weights into the single space of function values are introduced in the IRBFN approach, thereby keeping the system matrix size small and comparable to that associated with the DRBFN approach. Furthermore, the nonlinear systems of equations obtained are solved with the use of trust region methods. The present approach yields very good results using relatively low numbers of data points. For example, in the simulation of driven cavity viscous flows, a high Reynolds number of 3200 is achieved using only 51×51 data points.

Keywords radial basis function, trust region methods, Poisson equation, Navier-Stokes equations, driven cavity viscous flow.

1 Introduction

The finite difference method (FDM) (cf. [2]), the finite element method (FEM) (cf. [3]), the finite volume method (FVM) (cf. [4]) and the boundary element method (BEM) (cf. [5,6]) are powerful techniques for numerical solution of boundary-value problems in continuum mechanics. Each method has some advantages over the others in certain classes of problems. They have achieved a lot of success in solving engineering and science problems. However, since their approximations to the governing equations and boundary conditions are usually based on low order schemes such as constant, linear and quadratic ones, dense meshes are required for a high degree of accuracy. On the other hand, the spectral method (cf. [7,8]), the differential quadrature method (cf. [9]) and the radial basis function network (RBFN) based method (cf. [10]) fall under the category of high order methods by which accurate results can be obtained using relatively coarse discretizations of the domain of interest.

The concept of solving PDEs by using RBFNs was first introduced by Kansa [10]. A further distinguishing feature of the methods based on the neural network methodology is that no mesh is required. The methods use approximators based on RBFNs to represent the solution via a point collocation mechanism. The difference between the RBFN and spectral collocation methods is that collocation points are chosen as the roots of the base functions (Chebychev polynomials) for the latter but can be chosen randomly for the former. In this sense, RBFNs are comparatively easy to implement especially for problems with complex geometries or with governing differential equations involving complicated operators. It has been proven that RBFNs with one hidden layer are capable of universal approximation [11,12]. Although RBFNs have the ability to represent any continuous function to a prescribed degree of accuracy, practical means to acquire sufficient approximation accuracy still

remain an open problem. For example, due to the lack of theory, it is still very difficult to choose the optimum values of RBFN parameters such as the RBF's widths (shape parameters), which are seen to critically affect the performance of RBFNs. That could be a reason why the RBFN-based methods have not been extensively used to solve practical problems.

In an RBFN-based method, each dependent variable and its derivatives are expressed as linear combinations of basis functions which are associated with the same set of network weights. There are two basic approaches for obtaining new basis functions from RBFs. The first approach, namely the direct RBFNs (DRBFNs), is based on a differentiation process [10], while the second approach, namely the indirect RBFNs (IRBFNs), is based on an integration process [1]. The two approaches were tested with the solution of elliptic DEs and the IRBFN method was found to be more tolerant than the DRBFN method in the choice of the RBF's widths [1]. The IRBFN method was then extended successfully to simulate the driven cavity viscous flows with the Reynolds number achieved up to 400 using a uniform set of 33×33 data points [13]. A formal theoretical proof of the superior accuracy of the IRBFN method has not been given at this stage. However, a heuristic argument can be presented as follows. In the direct approach, the starting point is the decomposition of the original function into some finite basis and all derivatives are subsequently obtained by differentiation. Any inaccuracy in the assumed decomposition is badly magnified in the process of differentiation. In contrast, in the indirect approach, the starting point is the decomposition of the highest derivatives into some finite basis. Lower derivatives and finally the function itself are obtained by integration which has the property of damping out or at least containing any inherent inaccuracy in the assumed shape of the derivatives.

A disadvantage of the IRBFN approach is that when the problem dimensionality N is greater than 1, the size of the system of equations obtained in the IRBFN approach

is about N times as big as that in the DRBFN approach. **The increase in size of the unknown network weights in the indirect approach is primarily due to the fact that there are N radial basis function networks associated with N coordinates to be used in representing each dependent variable and its derivatives. Consequently, some additional constraints are necessary to make the formal function representations identical** [1]. In this paper, the multiple spaces of network weights, which are unknowns here, are converted into the single space of function values, resulting in a square system of equations with usual size and hence greatly reducing computational effort and storage for the IRBFN method.

For nonlinear problems, it is well known that the Newton iteration method is often used for efficient convergence of a numerical scheme. The method possesses local q-quadratic convergence provided that an initial guess for the iteration is close to the desired solution. In the case that the iteration process is not started sufficiently close to the desired solution, the Newton method needs be hybridized with a globally, yet typically slowly, convergent Cauchy method (steepest descent) in order to construct a globally convergent variant. The resulting so-called model-trust region algorithms retain the best features of both methods: strong global convergence coupled with rapid local convergence (i.e. they are globally q-quadratically convergent) [14]. In the present work, the trust region methods are applied to solve the obtained systems of nonlinear equations.

The present method is verified successfully through the solution of Poisson equation and the Navier-Stokes equations. For the case of Poisson equation, highly accurate results and fast convergence are obtained. For the case of the Navier-Stokes equations, in which the benchmark problem of viscous flow in a lid-driven cavity is simulated, the present approach yields solutions for high Reynolds numbers up to 3200 using relatively low numbers of data points. In the context of the solution of

the Navier-Stokes equations using RBF networks, this paper appears to be the first reporting the achievement of high Reynolds number solutions.

The remainder of the paper is organized as follows. Section 2 gives brief reviews of RBFNs and two associated DRBFN and IRBFN approaches. A new feature for the IRBFN approach is presented in section 3. The governing equations are given in section 4. Sections 5 & 6 discuss respectively the use of RBFNs for numerical solution of PDEs and the use of trust region methods for solving nonlinear algebraic systems. In section 7, the present IRBFN approach is verified through the solution of linear heat transfer problems with the Dirichlet and Neumann boundary conditions and the solution of non-zero Reynolds number viscous flows in a driven cavity. Section 8 gives some concluding remarks.

2 Radial Basis Function Networks

A function y to be approximated can be represented by an RBFN as follows [15]

$$y(\mathbf{x}) \approx f(\mathbf{x}) = \sum_{i=1}^{m} w^{(i)} g^{(i)}(\mathbf{x}), \tag{1}$$

where superscripts denote elements of a set of neurons, $\mathbf{x}$ is the input vector, m the number of RBFs, $\{w^{(i)}\}_{i=1}^{m}$ the set of network weights and $\{g^{(i)}(\mathbf{x})\}_{i=1}^{m}$ the set of RBFs. Since multiquadrics (MQ) are ranked the best in terms of accuracy among RBFs [16], the present work will employ these basis functions whose form is

$$g^{(i)}(\mathbf{x}) = \sqrt{(\mathbf{x} - \mathbf{c}^{(i)})^T (\mathbf{x} - \mathbf{c}^{(i)}) + a^{(i)2}}, \tag{2}$$

where $\mathbf{c}^{(i)}$ and $a^{(i)}$ are the centre and the width of the ith MQ basis function respectively and T denotes the transpose of a vector. To make the training process

simple, the centres and the widths of RBFs are chosen in advance. For the latter, the following relation is used

$$a^{(i)} = \beta d^{(i)}, \tag{3}$$

where β is a positive scalar and $d^{(i)}$ is the minimum of distances from the ith center to its neighbours.

The function y is now expressed as a weighted linear combination of radial basis functions. It can be seen that differentiating or integrating y also results in weighted linear combinations of basis functions, where the sets of network weights are identical.

2.1 Direct approach

In this approach, the RBF network (1) is utilized to represent the original function y and subsequently its derivatives are computed by differentiating (1) as follows

$$y(\mathbf{x}) \approx f(\mathbf{x}) = \sum_{i=1}^{m} w^{(i)} g^{(i)}(\mathbf{x}), \tag{4}$$

$$\frac{\partial y(\mathbf{x})}{\partial x_j} \approx \frac{\partial f(\mathbf{x})}{\partial x_j} = \frac{\partial \left(\sum_{i=1}^{m} w^{(i)} g^{(i)}(\mathbf{x})\right)}{\partial x_j} = \sum_{i=1}^{m} w^{(i)} h^{(i)}(\mathbf{x}), \tag{5}$$

$$\frac{\partial^2 y(\mathbf{x})}{\partial x_j^2} \approx \frac{\partial^2 f(\mathbf{x})}{\partial x_j^2} = \frac{\partial \left(\sum_{i=1}^{m} w^{(i)} h^{(i)}(\mathbf{x})\right)}{\partial x_j} = \sum_{i=1}^{m} w^{(i)} \bar{h}^{(i)}(\mathbf{x}), \tag{6}$$

where subscripts denote scalar components of a vector, $h^{(i)}(\mathbf{x}) = \partial g^{(i)}(\mathbf{x})/\partial x_j$ and $\bar{h}^{(i)}(\mathbf{x}) = \partial h^{(i)}(\mathbf{x})/\partial x_j$ are new derived basis functions in the approximation of first and second order derivatives of y respectively.

2.2 Indirect approach

In this approach, RBFNs are used to represent the highest order derivatives of a function y, e.g. $\partial^2 y/\partial x_1^2$ and $\partial^2 y/\partial x_2^2$. Lower order derivatives and finally the function itself are then obtained by integrating those RBFNs as follows

$$\frac{\partial^2 y(\mathbf{x})}{\partial x_j^2} \approx \frac{\partial^2 f(\mathbf{x})}{\partial x_j^2} = \sum_{i=1}^{m} w^{(i)} g^{(i)}(\mathbf{x}), \tag{7}$$

$$\frac{\partial y(\mathbf{x})}{\partial x_j} \approx \frac{\partial f(\mathbf{x})}{\partial x_j} = \int \left(\sum_{i=1}^{m} w^{(i)} g^{(i)}(\mathbf{x}) \right) dx_j = \sum_{i=1}^{m+p_1} w^{(i)} H^{(i)}(\mathbf{x}), \tag{8}$$

$$y(\mathbf{x}) \approx f(\mathbf{x}) = \int \left(\sum_{i=1}^{m+p_1} w^{(i)} H^{(i)}(\mathbf{x}) \right) dx_j = \sum_{i=1}^{m+p_2} w^{(i)} \bar{H}^{(i)}(\mathbf{x}), \tag{9}$$

where p_1 and p_2 are the numbers of centres used to represent integration constants in the first and second derivatives ($\frac{\partial f(\mathbf{x})}{\partial x_j}$ and $\frac{\partial^2 f(\mathbf{x})}{\partial x_j^2}$) respectively ($p_2 = 2p_1$). For convenience, these centres and their associated basis functions are also denoted by the notations $w^{(i)}$ and $H^{(i)}$ ($\bar{H}^{(i)}$) respectively but with $i > m$. For example, in the case of 2D problems, the integration constants in the first derivative $\frac{\partial f(\mathbf{x})}{\partial x_j}$ is a function of the variable $x_{k(k \neq j)}$ only and can be approximated using the indirect RBFN approach as follows

$$\frac{d^2 C_1(x_k)}{dx_k^2} = \sum_{i=1}^{p_1-2} \bar{w}^{(i)} g^{(i)}(x_k), \tag{10}$$

$$\frac{dC_1(x_k)}{dx_k} = \sum_{i=1}^{p_1-2} \bar{w}^{(i)} H^{(i)}(x_k) + \widehat{C}_1 = \sum_{i=1}^{p_1-1} \bar{w}^{(i)} H^{(i)}(x_k), \tag{11}$$

$$C_1(x_k) = \sum_{i=1}^{p_1-2} \bar{w}^{(i)} \bar{H}^{(i)}(x_k) + \widehat{C}_1 x_k + \widehat{C}_2 = \sum_{i=1}^{p_1} \bar{w}^{(i)} \bar{H}^{(i)}(x_k), \tag{12}$$

where

$$\left\{H^{(i)}(x_k)\right\}_{i=1}^{p_1-2} = \left\{\int g^{(i)}(x_k)dx_k\right\}_{i=1}^{p_1-2},\ \left\{\bar{H}^{(i)}(x_k)\right\}_{i=1}^{p_1-2} = \left\{\int H^{(i)}(x_k)dx_k\right\}_{i=1}^{p_1-2},$$

$$H^{(p_1-1)}(x_k) = 1,\ \bar{H}^{(p_1-1)}(x_k) = x_k,\ \bar{H}^{(p_1)}(x_k) = 1,$$

$$\bar{w}^{(p_1-1)} = \widehat{C_1} \quad \text{and} \quad \bar{w}^{(p_1)} = \widehat{C_2}.$$

The detailed implementation was reported previously in [17]. **In the present work, the new centres in the approximation of integration constants (e.g. $C_1(x_k)$) are chosen to be distinct x_k coordinates of data points.**

Several basis functions in both DRBFN and IRBFN approaches are available in analytic forms and they can be found in [17].

3 New feature for the indirect approach

As reviewed above, in the indirect approach, the highest order derivatives are represented by RBFNs. Subsequently, lower order derivatives and the function are obtained by integrating the RBFNs. For the approximation of a function of two or more variables, there are a number of expressions obtained to represent a target function since different starting points can be employed by virtue of the definition of partial derivatives. Thus, it is necessary to impose some constraints on the function networks in order to make the formal function representations identical [1].

The indirect approach for 2D problems can be recaptured as follows

$$\frac{\partial^2 f(\mathbf{x})}{\partial x_1^2} \rightarrow \frac{\partial f(\mathbf{x})}{\partial x_1} \rightarrow f_{[x_1]}(\mathbf{x}), \tag{13}$$

$$\frac{\partial^2 f(\mathbf{x})}{\partial x_2^2} \rightarrow \frac{\partial f(\mathbf{x})}{\partial x_2} \rightarrow f_{[x_2]}(\mathbf{x}), \tag{14}$$

where $f_{[x_1]}(\mathbf{x})$ and $f_{[x_2]}(\mathbf{x})$ are two closed-form representations for the function y corresponding to the two starting points $\partial^2 f/\partial x_1^2$ and $\partial^2 f/\partial x_2^2$ respectively. Since $f_{[x_1]}(\mathbf{x})$ and $f_{[x_2]}(\mathbf{x})$ represent the same function, they must be identical, leading to the following constraint equation

$$f_{[x_1]}(\mathbf{x}) = f_{[x_2]}(\mathbf{x}) = f(\mathbf{x}). \tag{15}$$

Functions in (13)-(15) can be written as linear combinations of basis functions as follows

$$\sum_{i=1}^{m} g^{(i)}(\mathbf{x}) w_{[x_1]}^{(i)} \rightarrow \sum_{i=1}^{m+p_1} H_{[x_1]}^{(i)}(\mathbf{x}) w_{[x_1]}^{(i)} \rightarrow \sum_{i=1}^{m+p_2} \bar{H}_{[x_1]}^{(i)}(\mathbf{x}) w_{[x_1]}^{(i)}, \tag{16}$$

$$\sum_{i=1}^{m} g^{(i)}(\mathbf{x}) w_{[x_2]}^{(i)} \rightarrow \sum_{i=1}^{m+p_1} H_{[x_2]}^{(i)}(\mathbf{x}) w_{[x_2]}^{(i)} \rightarrow \sum_{i=1}^{m+p_2} \bar{H}_{[x_2]}^{(i)}(\mathbf{x}) w_{[x_2]}^{(i)}, \tag{17}$$

$$\sum_{i=1}^{m+p_2} \bar{H}_{[x_1]}^{(i)}(\mathbf{x}) w_{[x_1]}^{(i)} = \sum_{i=1}^{m+p_2} \bar{H}_{[x_2]}^{(i)}(\mathbf{x}) w_{[x_2]}^{(i)}, \tag{18}$$

where subscripts $[x_i]$ denote the results obtained by the integration with respect to the x_i direction. The evaluation of (16)-(18) at a set of collocation points $\{\mathbf{x}^{(j)}\}_{j=1}^n$ yields the system of equations of the form

$$\mathbf{f}_{,\mathbf{11}}(\mathbf{x}) = \mathbf{G}(\mathbf{x})\mathbf{w}_{[x_1]} \rightarrow \mathbf{f}_{,\mathbf{1}}(\mathbf{x}) = \mathbf{H}_{[x_1]}(\mathbf{x})\mathbf{w}_{[x_1]} \rightarrow \mathbf{f}_{[x_1]}(\mathbf{x}) = \bar{\mathbf{H}}_{[x_1]}(\mathbf{x})\mathbf{w}_{[x_1]}, \tag{19}$$

$$\mathbf{f}_{,\mathbf{22}}(\mathbf{x}) = \mathbf{G}(\mathbf{x})\mathbf{w}_{[x_2]} \rightarrow \mathbf{f}_{,\mathbf{2}}(\mathbf{x}) = \mathbf{H}_{[x_2]}(\mathbf{x})\mathbf{w}_{[x_2]} \rightarrow \mathbf{f}_{[x_2]}(\mathbf{x}) = \bar{\mathbf{H}}_{[x_2]}(\mathbf{x})\mathbf{w}_{[x_2]}, \tag{20}$$

$$\bar{\mathbf{H}}_{[x_1]}(\mathbf{x})\mathbf{w}_{[x_1]} = \bar{\mathbf{H}}_{[x_2]}(\mathbf{x})\mathbf{w}_{[x_2]}, \tag{21}$$

where $\mathbf{G}$, $\mathbf{H}$ and $\bar{\mathbf{H}}$ are the design matrices associated with the approximation of second derivative, first derivative and the function respectively; $\mathbf{w}_{[x_i]}$ the sets of network weights to be found; $\mathbf{f} = \{f(\mathbf{x}^{(j)})\}_{j=1}^n$; $\mathbf{f}_{,\mathbf{i}} = \{\frac{\partial f(\mathbf{x}^{(j)})}{\partial x_i}\}_{j=1}^n$ and $\mathbf{f}_{,\mathbf{ii}} = \{\frac{\partial^2 f(\mathbf{x}^{(j)})}{\partial x_i^2}\}_{j=1}^n$. For the convenience of computation, the matrices $\mathbf{G}$ and $\mathbf{H}$ are augmented using zero-submatrices so that they have the same size as the matrix $\bar{\mathbf{H}}$.

Obviously, the unknown vector in the indirect approach is $(\mathbf{w}_{[x_1]}; \mathbf{w}_{[x_2]}; \cdots; \mathbf{w}_{[x_N]})$ in which the length of each $\mathbf{w}_{[x_i]}$ is $(m + p_2)$ and N is the problem dimensionality. Assuming that p_2 (a number of additional weights from the approximation of integration constants) is a relatively small number, the size of the unknown vector in the original indirect RBFN approach is about N times as big as that in the direct RBFN approach.

This paper introduces prior conversions of the multiple spaces of network weights, e.g. $\mathbf{w}_{[x_1]}$ and $\mathbf{w}_{[x_2]}$, into the single space of function values $\mathbf{f}$ in order to form a square system of equations of smaller size (comparable to that associated with the DRBFN approach), thus greatly reducing the computational effort and storage. Consider the function networks $\mathbf{f}_{[x_1]}$ and $\mathbf{f}_{[x_2]}$ in (19) and (20) respectively. By inversion, the sets of network weights are expressed in terms of nodal function values as

$$\mathbf{w}_{[x_1]} = \bar{\mathbf{H}}^{-1}_{[x_1]}\mathbf{f}_{[x_1]} = \bar{\mathbf{H}}^{-1}_{[x_1]}\mathbf{f}, \tag{22}$$

$$\mathbf{w}_{[x_2]} = \bar{\mathbf{H}}^{-1}_{[x_2]}\mathbf{f}_{[x_2]} = \bar{\mathbf{H}}^{-1}_{[x_2]}\mathbf{f}. \tag{23}$$

Substitution of (22) and (23) into the system (19)-(20) yields

$$\mathbf{f}_{,\mathbf{11}} = \mathbf{G}\bar{\mathbf{H}}^{-1}_{[x_1]}\mathbf{f} \rightarrow \mathbf{f}_{,\mathbf{1}} = \mathbf{H}_{[x_1]}\bar{\mathbf{H}}^{-1}_{[x_1]}\mathbf{f} \rightarrow \mathbf{f}_{[x_1]} = \mathbf{I}\mathbf{f}, \tag{24}$$

$$\mathbf{f}_{,\mathbf{22}} = \mathbf{G}\bar{\mathbf{H}}^{-1}_{[x_2]}\mathbf{f} \rightarrow \mathbf{f}_{,\mathbf{2}} = \mathbf{H}_{[x_2]}\bar{\mathbf{H}}^{-1}_{[x_2]}\mathbf{f} \rightarrow \mathbf{f}_{[x_2]} = \mathbf{I}\mathbf{f}, \tag{25}$$

where $\mathbf{I}$ is the unit matrix.

For cross derivatives $\partial f^2(\mathbf{x})/\partial x_i \partial x_j$, it is straightforward to compute them by using network design matrices associated with first order derivatives. Although the order of differentiation makes no difference theoretically, due to numerical error, it would

be better to take the average of the two equivalent representations

$$\begin{aligned}\frac{\partial^2 f}{\partial x_i \partial x_j} &= \frac{1}{2}\left(\frac{\partial}{\partial x_i}\left(\frac{\partial f}{\partial x_j}\right)+\frac{\partial}{\partial x_j}\left(\frac{\partial f}{\partial x_i}\right)\right),\\ \mathbf{f_{,ij}} &= \frac{1}{2}\left(\mathbf{H}_{[x_i]}\bar{\mathbf{H}}^{-1}_{[x_i]}\left(\mathbf{H}_{[x_j]}\bar{\mathbf{H}}^{-1}_{[x_j]}\mathbf{f}\right)+\mathbf{H}_{[x_j]}\bar{\mathbf{H}}^{-1}_{[x_j]}\left(\mathbf{H}_{[x_i]}\bar{\mathbf{H}}^{-1}_{[x_i]}\mathbf{f}\right)\right). \qquad (26)\end{aligned}$$

It can be seen from (24)-(26) that the function and its derivatives are all expressed in terms of the function values rather than in terms of the network weights. **As a result, the system of equations obtained is normally square with the size being slightly smaller than that of the DRBFN method, irrespective of the problem dimensionality. For example, in solving Poisson equation, the sizes of the system matrices are $nip \times nip$ and $n \times n$ for the indirect and direct approaches respectively in which nip is the number of interior points and n the number of boundary and interior points.** The transformation operation completely eliminates the problem of large matrix size in the IRBFN method.

4 Governing equations

Linear Poisson equations and nonlinear Navier-Stokes equations are considered in the present work.

4.1 Poisson equation

The linear Poisson equation takes the form

$$\frac{\partial^2 u}{\partial x_1^2}+\frac{\partial^2 u}{\partial x_2^2}=s(\mathbf{x}), \qquad \mathbf{x}\in\Omega \qquad (27)$$

where $\mathbf{x} = (x_1, x_2)$ is the position vector of a point in the analysis domain Ω, u is the dependent variable and s is a known function.

4.2 The Navier-Stokes equations

In solving the Navier-Stokes equations for two dimensional flows, numerical methods usually employ the stream function-vorticity formulation rather than the velocity-pressure formulation. The advantages of the former over the latter are that the number of variables is reduced to two (without pressure) and the continuity equation is automatically satisfied. However, one concern is the need to derive boundary conditions for the vorticity. The stream function-vorticity formulation will be employed here. The dimensionless Navier-Stokes equations for steady incompressible planar viscous flows, subject to negligible body forces, are expressible in terms of the stream function ϕ and the vorticity ω as follows

$$\frac{\partial^2 \phi}{\partial x_1^2} + \frac{\partial^2 \phi}{\partial x_2^2} + \omega = 0, \qquad \mathbf{x} \in \Omega \tag{28}$$

$$\frac{\partial^2 \omega}{\partial x_1^2} + \frac{\partial^2 \omega}{\partial x_2^2} = Re \left(\frac{\partial \phi}{\partial x_2} \frac{\partial \omega}{\partial x_1} - \frac{\partial \phi}{\partial x_1} \frac{\partial \omega}{\partial x_2} \right) \qquad \mathbf{x} \in \Omega, \tag{29}$$

where $Re = UL/\nu$ is the Reynolds number, in which L is the characteristic length, U is the characteristic speed of the flow and ν is the kinematic viscosity. The vorticity and stream function are defined by

$$\omega = \frac{\partial u_2}{\partial x_1} - \frac{\partial u_1}{\partial x_2}, \tag{30}$$

$$\frac{\partial \phi}{\partial x_2} = u_1, \quad \frac{\partial \phi}{\partial x_1} = -u_2, \tag{31}$$

where u_1 and u_2 are the components of the velocity vector.

5 Solution of PDEs using RBFNs

Each variable and its derivatives in the governing equations can be represented by neural networks using either (4)-(6) in the direct approach or (24)-(25) in the indirect approach. The closed-form representations obtained are then substituted into the governing equations and boundary conditions to discretize the system via a point collocation mechanism. In the present work, the set of collocation points is chosen to be the same as the set of centres, i.e. $\{\mathbf{x}^{(i)}\}_{i=1}^{n} = \{\mathbf{c}^{(i)}\}_{i=1}^{m}$. The RBFN solution satisfies the governing equations pointwise rather than in an average sense. In order to form a square system, the governing equations are applied to the interior points only.

In the indirect approach, the unknown vector contains nodal variable values, e.g. u in Poisson equation and $\{\phi, \omega\}$ in the Navier-Stokes equations, while in the direct approach, the unknowns are the network weights (coefficients). However, for both approaches, it can be seen that the determination of the unknowns is based on the process of minimizing the following sum squared errors SSE

$$SSE = SSE_1 + SSE_2, \tag{32}$$

where SSE_1 and SSE_2 are the sums of squared errors, which are employed to ensure that neural networks satisfy the governing equations and the boundary conditions respectively. The form of SSE_2 depends on the problem to be solved while the term SSE_1 can be written in the general form provided that the governing equations are given. For example, SSE_1 in the IRBFN formulation takes the form

$$SSE_1 = \sum_{i=1}^{nip} \left[\sum_{j=1}^{m} \left(\mathbf{G}\bar{\mathbf{H}}_{[x_1]}^{-1} \right)_{[i,j]} u^{(j)} + \sum_{j=1}^{m} \left(\mathbf{G}\bar{\mathbf{H}}_{[x_2]}^{-1} \right)_{[i,j]} u^{(j)} - s(\mathbf{x}^{(i)}) \right]^2, \tag{33}$$

for Poisson equation (27) and

$$
\begin{aligned}
SSE_1 = & \sum_{i=1}^{nip}\{\sum_{j=1}^{m}\left(\mathbf{G}\bar{\mathbf{H}}^{-1}_{[x_1]}\right)_{[i,j]}\phi^{(j)} + \sum_{j=1}^{m}\left(\mathbf{G}\bar{\mathbf{H}}^{-1}_{[x_2]}\right)_{[i,j]}\phi^{(j)} + \omega^{(i)}]\}^2 + \\
& \sum_{i=1}^{nip}\{\sum_{j=1}^{m}\left(\mathbf{G}\bar{\mathbf{H}}^{-1}_{[x_1]}\right)_{[i,j]}\omega^{(j)} + \sum_{j=1}^{m}\left(\mathbf{G}\bar{\mathbf{H}}^{-1}_{[x_2]}\right)_{[i,j]}\omega^{(j)} - \\
& Re[\sum_{j=1}^{m}\left(\mathbf{H}_{[x_2]}\bar{\mathbf{H}}^{-1}_{[x_2]}\right)_{[i,j]}\phi^{(j)}\left(\mathbf{H}_{[x_1]}\bar{\mathbf{H}}^{-1}_{[x_1]}\right)_{[i,j]}\omega^{(j)} - \\
& \sum_{j=1}^{m}\left(\mathbf{H}_{[x_1]}\bar{\mathbf{H}}^{-1}_{[x_1]}\right)_{[i,j]}\phi^{(j)}\left(\mathbf{H}_{[x_2]}\bar{\mathbf{H}}^{-1}_{[x_2]}\right)_{[i,j]}\omega^{(j)}]\}^2, \qquad (34)
\end{aligned}
$$

for the Navier-Stokes equations (28)-(29), where nip is the number of interior points and $[i, j]$ denotes the element located at the row i and the column j in a matrix.

In the context of meshless numerical methods, Atluri and Zhu [18] gave the definition of a truly meshless method. A method is regarded as a truly meshless method if both processes of interpolation (solution variables) and integration (e.g. integration of the weak form in FEM or integration of the inverse statement in BEM) are performed without using a mesh. Based on this definition, both direct and indirect RBFN approaches here are truly meshless methods as they use RBFNs and point collocation. The RBF networks just need a distribution of discrete points throughout a volume for the approximation and hence the need for discretization of the domain of interest into a number of elements is eliminated. Although there are some integration processes employed in the IRBFN method for the purpose of obtaining new basis functions from RBFs, no background meshes are required here since all integrals are obtained analytically.

It will be shown in the section on numerical examples that the IRBFN method is found to be considerably superior to the DRBFN method in both solution accuracy and convergence rate.

6 Nonlinear problems and trust region methods

Nonlinear problems lead to nonlinear systems of equations which must be solved iteratively. Two iterative techniques, namely the Picard iteration scheme and the Newton iteration scheme, are usually preferred to handle the nonlinearity of the system. In computational fluid dynamics, there is a body of evidence to indicate that the latter is more powerful than the former. The Newton algorithm converges quadratically while the Picard algorithm is often slow. Furthermore, it has been reported, for example in the BEM literature, that the Picard iteration scheme is appropriate only for low Reynolds number flows and beyond that range, the use of a Newton-Raphson type algorithm is imperative [19].

It should be noted that the Newton iteration's convergence is not guaranteed in cases where the starting point is far from the solution and the Jacobian matrix is ill conditioned. Fortunately, trust region techniques improve robustness when dealing with these difficult situations and will be applied in the present work.

In the trust region algorithm, the objective function at the current point is approximated by a simpler function such as a quadratic model in a neighbourhood around that point. The size of the neighbourhood (trust region) is controlled according to how well the local model reflects the behaviour of the objective function. The subproblem is thus formulated from which the search direction can be found by minimizing a local model, leading to a new point with a lower function value. The details are as follows.

The final system of nonlinear equations obtained from discretizing the governing equations and boundary conditions can be written in a matrix form as follows

$$\mathbf{A}(\mathbf{x}) = \mathbf{0}. \tag{35}$$

One approach to solve this problem is to convert the root-finding problem (35) into the unconstrained minimization problem, i.e. minimizing the Euclidean norm of the residual of the system of equations

$$\min_{\mathbf{x}} \mathbf{q}(\mathbf{x}) = \frac{1}{2}\mathbf{A}(\mathbf{x})^T\mathbf{A}(\mathbf{x}). \tag{36}$$

In the vicinity of the current point $\bar{\mathbf{x}}$, the trust region methods approximate the function $\mathbf{q}$ with a simpler function $\mathbf{m}$ by using a second order Taylor series expansion

$$\mathbf{m} = \frac{1}{2}\mathbf{A}(\bar{\mathbf{x}})^T\mathbf{A}(\bar{\mathbf{x}}) + [\mathbf{J}(\bar{\mathbf{x}})^T\mathbf{A}(\bar{\mathbf{x}})]^T\mathbf{d} + \frac{1}{2}\mathbf{d}^T[\mathbf{J}(\bar{\mathbf{x}})^T\mathbf{J}(\bar{\mathbf{x}})]^T\mathbf{d} \tag{37}$$

$$= \frac{1}{2}\left(\mathbf{A}(\bar{\mathbf{x}}) + \mathbf{J}(\bar{\mathbf{x}})\mathbf{d}\right)\left(\mathbf{A}(\bar{\mathbf{x}}) + \mathbf{J}(\bar{\mathbf{x}})\mathbf{d}\right)^T \qquad \|\mathbf{D}.\mathbf{d}\| \leq \Delta, \tag{38}$$

where $\mathbf{d}$ is the search direction, $\mathbf{J}(\bar{\mathbf{x}})$ is the Jacobian matrix, $\mathbf{D}$ is the unit matrix or a diagonal matrix and Δ is a positive scalar (trust region radius). The value of Δ is adjusted to ensure that the function $\mathbf{m}$ obtained represents $\mathbf{q}$ adequately. Note that the local quadratic model $\mathbf{m}(\mathbf{d})$ is a better choice of merit function than $\mathbf{q}$. The trust region subproblem is formulated as

$$\min_{\mathbf{d}} \mathbf{m} \qquad \|\mathbf{D}.\mathbf{d}\| \leq \Delta, \tag{39}$$

which can be solved efficiently using a dogleg strategy, resulting in the direction of search $\mathbf{d}$. Since the gradients of $\mathbf{q}$ and $\mathbf{m}$ are identical at $\bar{\mathbf{x}}$, they share descent directions from that point (global convergence property). Further details of the trust region methods can be found in [14,20,21]. The procedure used was provided in MATLAB (Release 13) package.

7 Numerical examples

In the following numerical examples, for simplicity, the width of the ith RBF is chosen to be the minimum distance from the ith centre to its neighbours, i.e. $\beta = 1$. Furthermore, the set of centres and the set of collocation points are taken to be the same ($m = n$). Illustrative examples include linear heat transfer and nonlinear viscous flow problems.

7.1 Heat transfer problems

Poisson equations with the Dirichlet and Neumann boundary conditions are considered. The DRBFN approach is also employed to provide the basis for the assessment of the presently proposed IRBFN approach. Since analytic solutions are available here, the accuracy of the solution obtained is measured via the norm of relative errors of the solution as follows

$$N_e = \sqrt{\frac{\sum_{i=1}^{n} \left[u_e(x^{(i)}) - u(x^{(i)})\right]^2}{\sum_{i=1}^{n} u_e(x^{(i)})^2}}, \tag{40}$$

where u and u_e are the calculated and exact solutions respectively and n is the number of collocation points.

7.1.1 Poisson equation with a Dirichlet boundary condition

The problem here is to determine a function $u(x_1, x_2)$ satisfying the following PDE

$$\frac{\partial^2 u}{\partial x_1^2} + \frac{\partial^2 u}{\partial x_2^2} = \sin(\pi x_1)\sin(\pi x_2) \tag{41}$$

defined on the rectangle $0 \leq x_1 \leq 1, \quad 0 \leq x_2 \leq 1$, subject to the Dirichlet condition $u = 0$ along the whole boundary of the domain. The exact solution is given by

$$u_e(x_1, x_2) = -\frac{1}{2\pi^2} \sin(\pi x_1) \sin(\pi x_2). \tag{42}$$

Five data sets of 10×10, 20×20, 31×31, 41×41 and 51×51 uniformly distributed data points are employed to verify the present method. In the IRBFN approach, it is straightforward to impose a Dirichlet boundary condition since the variable and its derivatives are expressed in terms of nodal function values. In the DRBFN approach, collocation points along the boundaries are used to enforce the boundary condition requirement. For both approaches, the obtained systems are square. Results are displayed in Figure 1, indicating that the IRBFN approach is superior to the DRBFN in terms of accuracy and convergence rate. Highly accurate results and high rates of convergence with "mesh" refinement are obtained with the present method. The solution converges apparently as $O(h^{3.4717})$ for IRBFN and $O(h^{1.3563})$ for DRBFN, where h is the centre spacing. At the finest density of 51×51, the error-norms are $2.0e-6$ and $2.8e-3$ for IRBFN and DRBFN respectively.

7.1.2 Poisson equation with both Dirichlet and Neumann conditions

In this example, the boundary conditions of the problem include both Dirichlet and Neumann type. Consider the following PDE

$$\frac{\partial^2 u}{\partial x_1^2} + \frac{\partial^2 u}{\partial x_2^2} = (\lambda^2 + \mu^2) \exp(\lambda x_1 + \mu x_2) \tag{43}$$

on the square domain ($0 \leq x_1 \leq 1,\ 0 \leq x_2 \leq 1$) with the following boundary conditions

$$u = \exp(\lambda x_1 + \mu x_2), \quad x_2 = 0 \quad \text{and} \quad x_2 = 1, \tag{44}$$

$$\frac{\partial u}{\partial x_1} = \lambda \exp(\lambda x_1 + \mu x_2), \quad x_1 = 0 \quad \text{and} \quad x_1 = 1. \tag{45}$$

The exact solution to the above problem is

$$u_e(x_1, x_2) = \exp(\lambda x_1 + \mu x_2). \tag{46}$$

Here, λ and μ are chosen to be 2 and 3, respectively. Special attention here is given to the treatment for the Neumann condition $\partial u/\partial n$. The present method implements this type of boundary condition as follows. Along the left ($x_1 = 0$) and right ($x_1 = 1$) sides of the domain, normal derivatives $\partial u/\partial n$ are given and hence the task now is to express the boundary values of u there in terms of the interior variable values. This can be achieved by solving the following subsystem of equations

$$\frac{\partial u(\mathbf{x}^{(i)})}{\partial x_1} = \sum_{j=1}^{m} \left(\mathbf{H}_{[x_1]} \bar{\mathbf{H}}^{-1}_{[x_1]} \right)_{[i,j]} u^{(j)}, \tag{47}$$

where $\mathbf{x}^{(i)} = \{(x_1 = 0, x_2), (x_1 = 1, x_2)\}$. Substitution of the results obtained from (47) and the Dirichlet condition (44) into the final system of equations yields a square system with the unknowns being only the interior variable values. Once the final system of equations is solved, the numerical solution u along two vertical sides may be found from (47). Figure 2 displays results obtained by the DRBFN and IRBFN approaches. The latter yields more accurate results and higher convergence rates than the former. At the finest density of 51×51, the error-norms are 1.2e-5 for IRBFN and 3.4e-2 for DRBFN. The IRBFN solution converges apparently as $O(h^{2.4129})$ while the DRBFN solution apparently as $O(h^{0.6877})$, where h is the centre spacing.

7.2 Viscous flow

The benchmark problem of steady viscous flow in an unitary square cavity [22] is simulated here to verify the present method. The fluid velocities on the left, right and bottom walls are fixed at zero, while the top non-slip solid driving lid is represented by a uniform non-zero velocity in the x_1-direction along the top edge (Figure 3). This problem is geometrically simple and has been used for decades as a standard test problem to verify and validate numerical methods in computational science and engineering. Ghia et al [23] provided a benchmark solution that is often cited for comparison purposes.

It is noted that the moving lid introduces stress singularities at the two top corners. At the upper corners, the velocity is discontinuous and the vorticity is unbounded.

The no-slip velocity conditions on the left, right and bottom walls ensure that

$$\phi = 0, \qquad \frac{\partial \phi}{\partial n} = 0, \tag{48}$$

while the uniform velocity of 1 along the top wall results in

$$\phi = 0, \qquad \frac{\partial \phi}{\partial n} = 1, \tag{49}$$

where n is the local direction normal to the wall. In the present work, the Poisson equation for ϕ (28) and the vorticity transport equation (29) are solved simultaneously in a coupled manner.

In the case of Poisson equation $\nabla^2 u = s$ with a Neumann boundary condition $(\partial u/\partial n)$, it is known that the solution will exist only when the following compatibility condition is fulfilled

$$\int_\Gamma \nabla u.\mathbf{n} d\Gamma = \int_\Omega s d\Omega, \tag{50}$$

where Γ denotes the boundary of the domain Ω. Even though equation (50) may be fulfilled, the singular nature of the system of equations will present additional complications [24]. Therefore, the direct employment of the Neumann condition $\partial\phi/\partial n$ over all boundaries via a point collocation mechanism is not appropriate here. Instead, it is used in generating a computational boundary condition for ω. The process is as follows. In the first step, the vorticity in (28) can be simplified to be

$$\omega = -\frac{\partial^2\phi}{\partial x_1^2} - \frac{\partial^2\phi}{\partial x_2^2} = -\frac{\partial^2\phi}{\partial x_1^2} \qquad \text{at the side walls,} \tag{51}$$

$$\omega = -\frac{\partial^2\phi}{\partial x_1^2} - \frac{\partial^2\phi}{\partial x_2^2} = -\frac{\partial^2\phi}{\partial x_2^2} \qquad \text{at the top and bottom walls,} \tag{52}$$

using the given boundary conditions. In the second step, they are written in terms of first order derivatives of ϕ

$$\omega^{(i)} = -\frac{\partial^2\phi^{(i)}}{\partial x_1^2} = \sum_{j=1}^{m} \left(\mathbf{G}\mathbf{H}_{[x_1]}^{-1}\right)_{[i,j]} \frac{\partial\phi}{\partial x_1}^{(j)} \qquad \text{at the side walls,} \tag{53}$$

$$\omega^{(i)} = -\frac{\partial^2\phi^{(i)}}{\partial x_2^2} = \sum_{j=1}^{m} \left(\mathbf{G}\mathbf{H}_{[x_2]}^{-1}\right)_{[i,j]} \frac{\partial\phi}{\partial x_2}^{(j)} \qquad \text{at the top and bottom walls,} \tag{54}$$

and the resulting expressions (53) and (54) are then simplified by taking into consideration the Neumann condition for ϕ ($\partial\phi/\partial n$). In the third step, the remainders of the nodal first derivatives of ϕ on the right-hand sides of (53) and (54) are expressed in terms of the nodal stream function values, for example at the boundary point $\mathbf{x^{(i)}}$,

$$\frac{\partial\phi}{\partial x_1}^{(i)} = \sum_{j=1}^{m} \left(\mathbf{H}_{[x_1]}\bar{\mathbf{H}}_{[x_1]}^{-1}\right)_{[i,j]} \phi^{(j)}, \tag{55}$$

$$\frac{\partial\phi}{\partial x_2}^{(i)} = \sum_{j=1}^{m} \left(\mathbf{H}_{[x_2]}\bar{\mathbf{H}}_{[x_2]}^{-1}\right)_{[i,j]} \phi^{(j)}. \tag{56}$$

Hence, the computational Dirichlet boundary condition for ω is generated and writ-

ten in terms of the nodal values of ϕ. It is noted that in this process, the natural boundary condition for the stream function is implemented in a precise manner.

The procedural flow chart involves the following steps

1. Input data such as geometries, boundary conditions, a Reynolds number and data points including a set of centres and a set of collocation points,
2. Apply the IRBFN approach for the approximation of each variable and its derivatives present in the relevant PDEs, which results in design matrices in the network weight spaces. It is noted that these matrices are the same for all variables,
3. Convert the multiple spaces of network weights into the single space of the primary variable values,
4. Generate a computational Dirichlet boundary condition for ω corresponding to the given Neumann boundary conditions,
5. Form the design matrix of the system, which involves only linear terms in the governing equations (28) and (29), and then impose the Dirichlet conditions for ϕ and ω. This matrix stays the same during the iteration process,
6. Initialize the stream function field and the vorticity field,
7. Compute the nonlinear convected vorticity terms, in which relevant derivative functions are calculated in a straightforward manner using the network design matrices obtained at step 3,
8. Formulate the trust region subproblem and then solve it for the search direction,
9. Update the solution,

10. Check for convergence. If not yet converged, repeat from step 7,

11. Output the results.

Four sets of 31×31, 41×41, 51×51 and 61×61 uniformly distributed data points are employed to study convergence. A range of Reynolds numbers $\{0, 400, 1000, 2000$ and $3200\}$ is considered. For the current Reynolds number, the solution for the previous value in the Reynolds number range is used as the initial solution and it takes about 10 iterations to achieve a convergence by using the trust region method. Another advantage of the trust region method over Picard-type iteration schemes is that no relaxation scheme is required and hence it requires less parametric study. Results obtained are in very good agreement with the benchmark solution of Ghia [23], which was found by the multigrid finite difference method using a mesh size of 129×129. For example, velocity profiles along the vertical and horizontal centrelines at some Reynolds numbers are displayed in Figures 4-6, where the IRBFN results are very close to those of Ghia [23] and "mesh" convergence is achieved (i.e. greater accuracy obtained with higher densities of data points used). Furthermore, in those figures, streamline patterns for the flows are also presented, which agree well with the benchmark solution.

Other important results are the properties of the primary vortex and the existence of secondary vortices at the corners. It can be seen that all secondary vortices are captured clearly, as shown in Figures 4-6. Several properties of the primary vortex such as the location and the minimum value of the stream function are given in the Table 1, showing that the present method yields a high degree of accuracy in the primary vortex region. It can be also seen from the table that IRBFN results are closer to the benchmark solution with an increase in data densities used (i.e. "mesh" convergence).

8 Concluding remarks

This paper reports an efficient IRBFN method for solution of PDEs. The approach differs from previous works in two aspects. The first one is that prior conversions of the multiple spaces of network weights into the single space of nodal variable values are introduced in order to form a square system of equations of smaller size, resulting in a great improvement in the performance of the indirect RBFN method. The second aspect is that the resulting nonlinear systems of equations are solved by the trust region methods, which are more robust than the Newton-Raphson type algorithms. The present method is truly meshless as no "finite element mesh" is required for the purpose of interpolation and integration. Numerical examples carried out in the paper show that accurate results and high rates of convergence with refinement of spatial discretisation are achieved using relatively coarse discretizations of the domain. This paper appears to be the first report achieving high Reynolds number solutions by RBFNs. A disadvantage of the present method is that the obtained system matrix is dense because the multiquadrics have non-local support and how to overcome this disadvantage is a topic currently under investigation.

Acknowledgements The authors are grateful to Prof. R.I. Tanner for many fruitful discussions. The authors would like to thank the referees for their helpful comments. The computing facilities provided by The APAC National Facility are gratefully acknowledged.

References

1. N. Mai-Duy and T. Tran-Cong, "Numerical solution of differential equations using multiquadric radial basis function networks," Neural Networks 14(2), 185 (2001).

2. P. J. Roache, Fundamentals of Computational Fluid Dynamics, Hermosa Pub-

lishers, Albuquerque, 1998.

3. O. C. Zienkiewicz and R. L. Taylor, The Finite Element Method, McGraw-Hill, London, 1991.

4. S. V. Patankar, Numerical Heat Transfer and Fluid Flow, McGraw-Hill, New York, 1980.

5. P. K. Banerjee and R. Butterfield, Boundary Element Methods in Engineering Science, McGraw-Hill, London, 1981.

6. C. A. Brebbia, J. C. F. Telles and L.C. Wrobel, Boundary Element Techniques Theory and Applications in Engineering, Springer-Velag, Berlin, 1984.

7. D. Gottlieb and S. A. Orszag, Numerical Analysis of Spectral Methods: Theory and Applications, SIAM, Philadelphia, 1977.

8. C. Bernardi and Y. Maday, "Spectral methods," in Handbook of Numerical Analysis, Vol. 5, P.G. Ciarlet and J.L. Lions (Editors), Elsevier Science, North Holland, 1997.

9. C. Shu, Differential Quadrature and Its Application in Engineering, Springer-Verlag, London, 2000.

10. E. J. Kansa, "Multiquadrics- A scattered data approximation scheme with applications to computational fluid-dynamics-II. Solutions to parabolic, hyperbolic and elliptic partial differential equations," Computers and Mathematics with Applications 19(8/9), 147 (1990).

11. J. Park and I. W. Sandberg, "Universal approximation using radial basis function networks," Neural Computation 3, 246 (1991).

12. J. Park and I. W. Sandberg, "Approximation and radial basis function networks," Neural Computation 5, 305 (1993).

13. N. Mai-Duy and T. Tran-Cong, "Numerical solution of Navier-Stokes equations using multiquadric radial basis function networks," International Journal for Numerical Methods in Fluids 37, 65 (2001).

14. B. J. McCartin, "A model-trust region algorithm utilizing a quadratic interpolant," Journal of Computational and Applied Mathematics 91, 249 (1998).

15. S. Haykin, Neural Networks: A Comprehensive Foundation, Prentice-Hall, New Jersey, 1999.

16. R. Franke, "Scattered data interpolation: tests of some methods," Mathematics of Computation 38(157), 181 (1982).

17. N. Mai-Duy and T. Tran-Cong, "Approximation of function and its derivatives using radial basis function network methods," Applied Mathematical Modelling 27, 197 (2003).

18. S. N. Atluri and T. Zhu, "New concepts in meshless methods," International Journal for Numerical Methods in Engineering 47, 537 (2000).

19. G. F. Dargush and P. K. Banerjee, "A boundary element method for steady incompressible thermoviscous flow," International Journal for Numerical Methods in Engineering 31, 1605 (1991).

20. J. J. More and D. C. Sorensen, "Computing a trust region step," SIAM Journal on Scientific and Statistical Computing 3, 553 (1983).

21. M. A. Branch , T. F. Coleman and Y. Li, "A subspace, interior and conjugate gradient method for large-scale bound-constrained minimization problems," SIAM Journal on Scientific Computing 21, 1 (1999).

22. P.J. Roache, Verification and Validation in Computational Science and Engineering, Hermosa Publishers, Albuquerque, 1998.

23. U. Ghia, K. N. Ghia and C. T. Shin, "High-Re solutions for incompressible flow using the Navier-Stokes equations and a multigrid method," Journal of Computational Physics 48, 387 (1982).

24. C. Pozrikidis, Introduction to Theoretical and Computational Fluid Dynamics, Oxford University Press, New York, 1997.

Table 1: Lid-driven cavity flow: some properties of the primary vortex

Density	Location		$\phi_{\min}$
	x_1	x_2	
$Re = 400$			
31×31	0.5555	0.6094	-0.1115
41×41	0.5547	0.6065	-0.1135
Benchmark	0.5547	0.6055	-0.1139
$Re = 1000$			
41×41	0.5316	0.5655	-0.1145
51×51	0.5315	0.5651	-0.1174
Benchmark	0.5313	0.5625	-0.1179
$Re = 3200$			
51×51	0.5199	0.5383	-0.1070
61×61	0.5195	0.5389	-0.1143
Benchmark	0.5165	0.5469	-0.1204

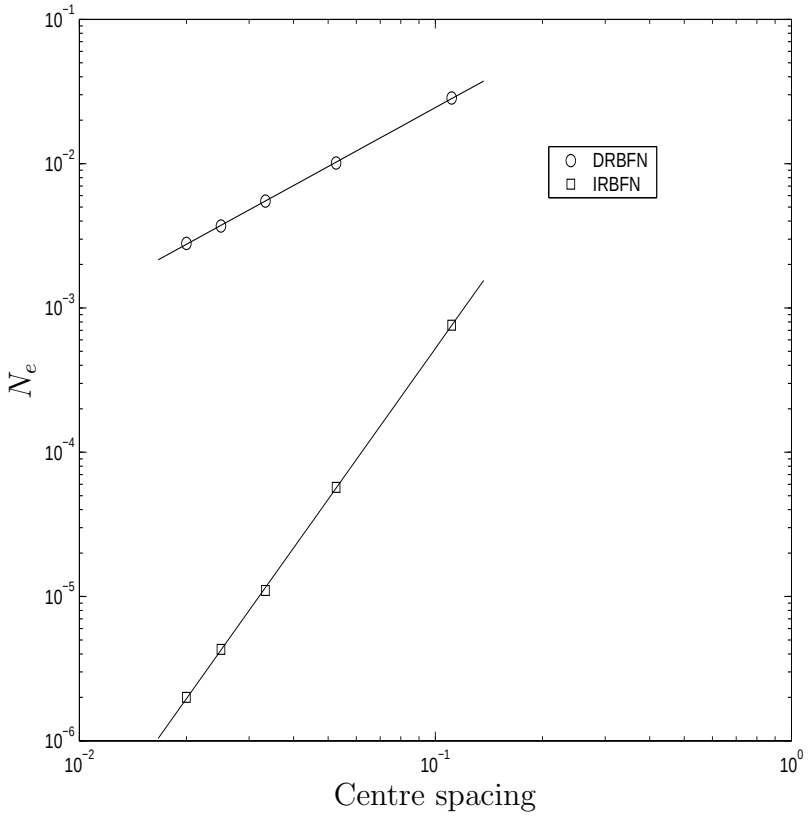

Figure 1: Poisson equation, Dirichlet boundary condition: Solution accuracy and convergence rate by the DRBFN and IRBFN methods. The solutions converge apparently as $O(h^{1.36})$ and $O(h^{3.47})$ for DRBFN and IRBFN respectively, where h is the centre spacing. The present IRBFN method possesses an excellent rate of convergence.

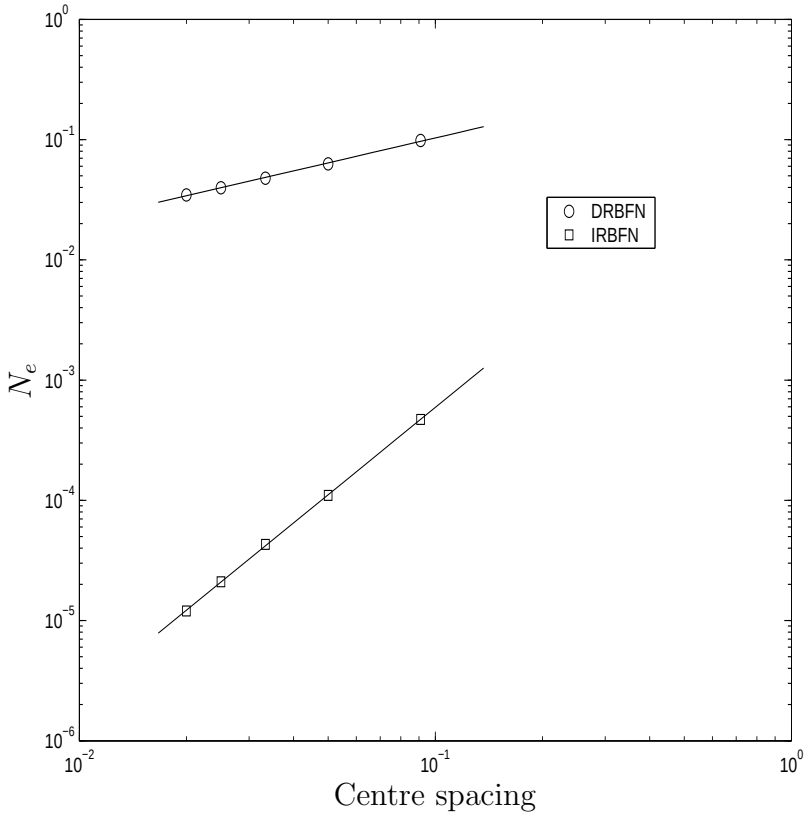

Figure 2: Poisson equation, Dirichlet and Neumann boundary conditions: Solution accuracy and convergence rate by the DRBFN and IRBFN methods. The solutions converge apparently as $O(h^{0.69})$ and $O(h^{2.41})$ for DRBFN and IRBFN respectively, where h is the centre spacing. The IRBFN method performs better than the DRBFN method in terms of both accuracy and convergence rate.

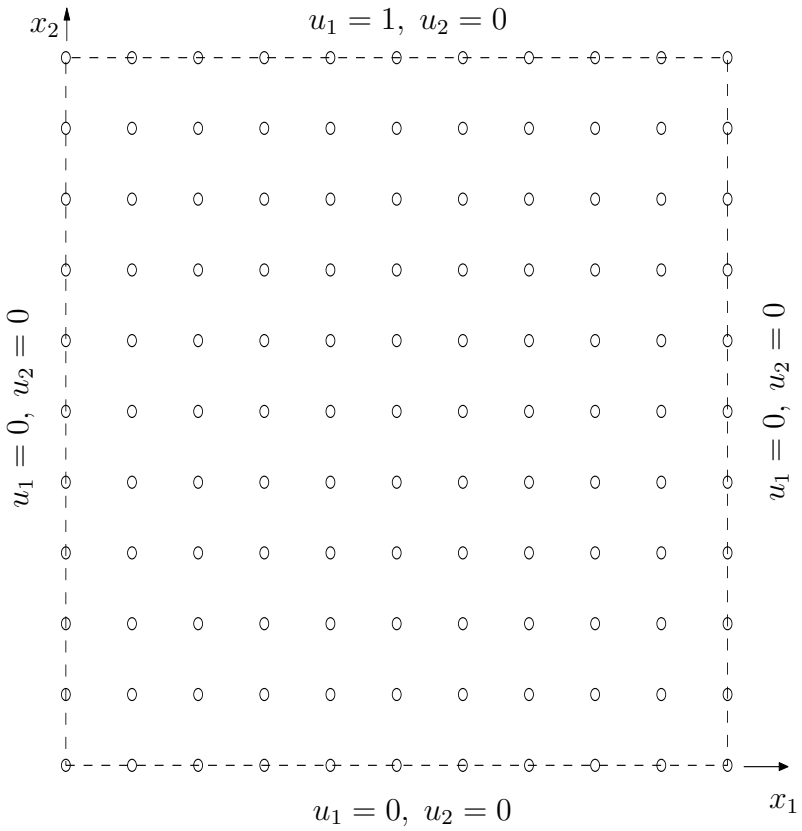

Figure 3: Lid-driven cavity viscous flow: geometry definition, boundary conditions and discretization. Legend ∘ denotes the centre/collocation point. The centre distribution is schematic only.

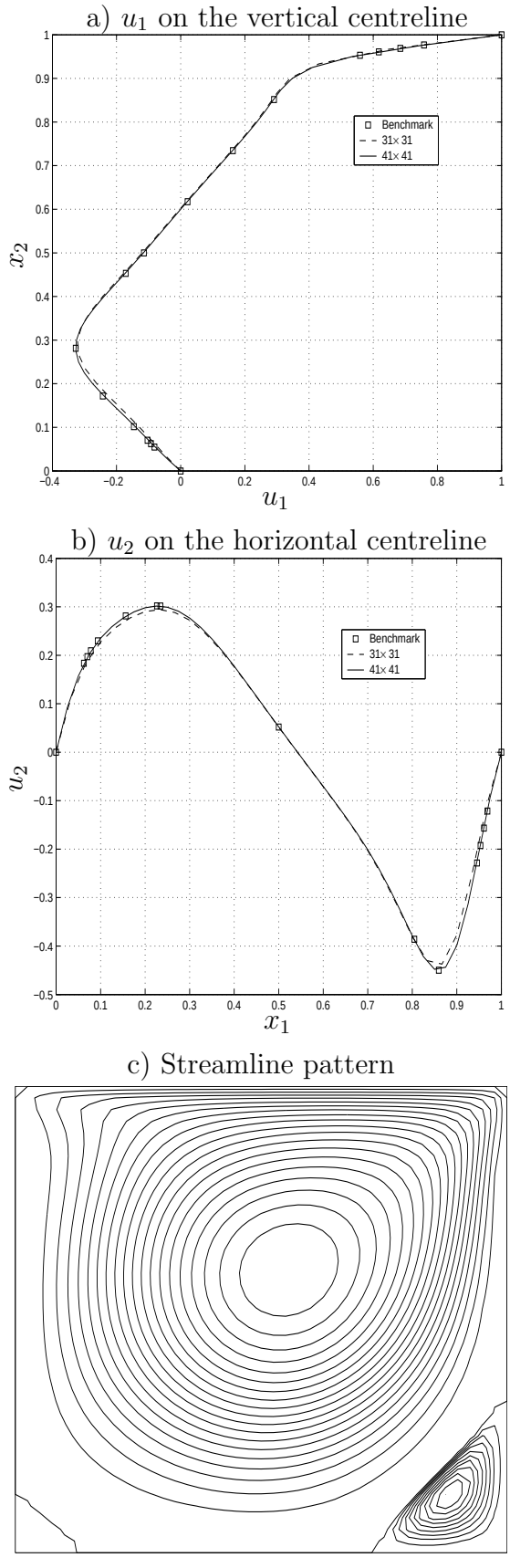

Figure 4: Driven cavity flow, $Re = 400$: Comparison of velocity profiles along the vertical and horizontal centrelines of the IRBFN method with the benchmark solution (Ghia et al [23] used 129×129 FD mesh). Higher densities of data points yield better accuracy. The streamline pattern obtained with a density of 41×41 is also displayed, where secondary vortices are clearly captured.

a) u_1 on the vertical centreline

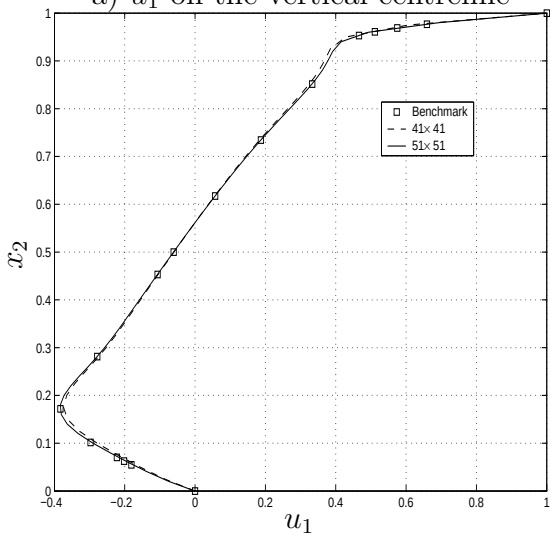

b) u_2 on the horizontal centreline

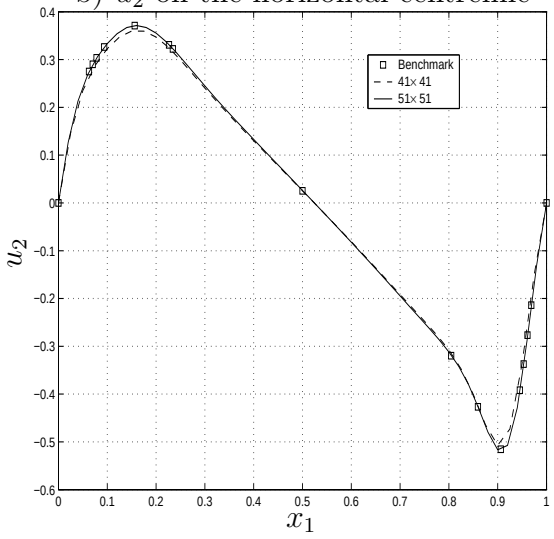

c) Streamline pattern

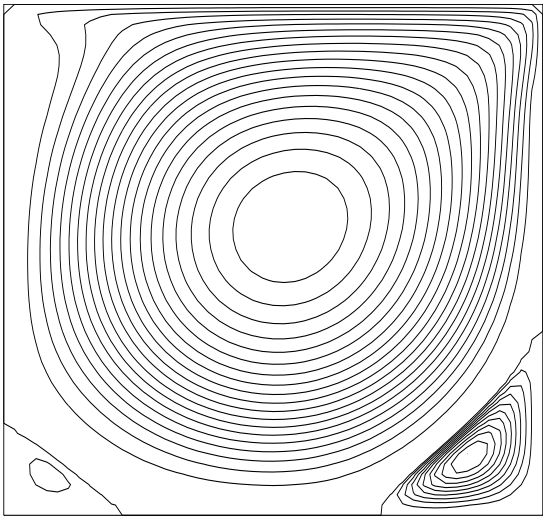

Figure 5: Driven cavity flow, $Re = 1000$: Comparison of velocity profiles along the vertical and horizontal centrelines of the IRBFN method with the benchmark solution (Ghia et al [23] used 129×129 FD mesh). Higher densities of data points yield better accuracy. The streamline pattern obtained with a density of 51×51 is also displayed, where secondary vortices are clearly captured.

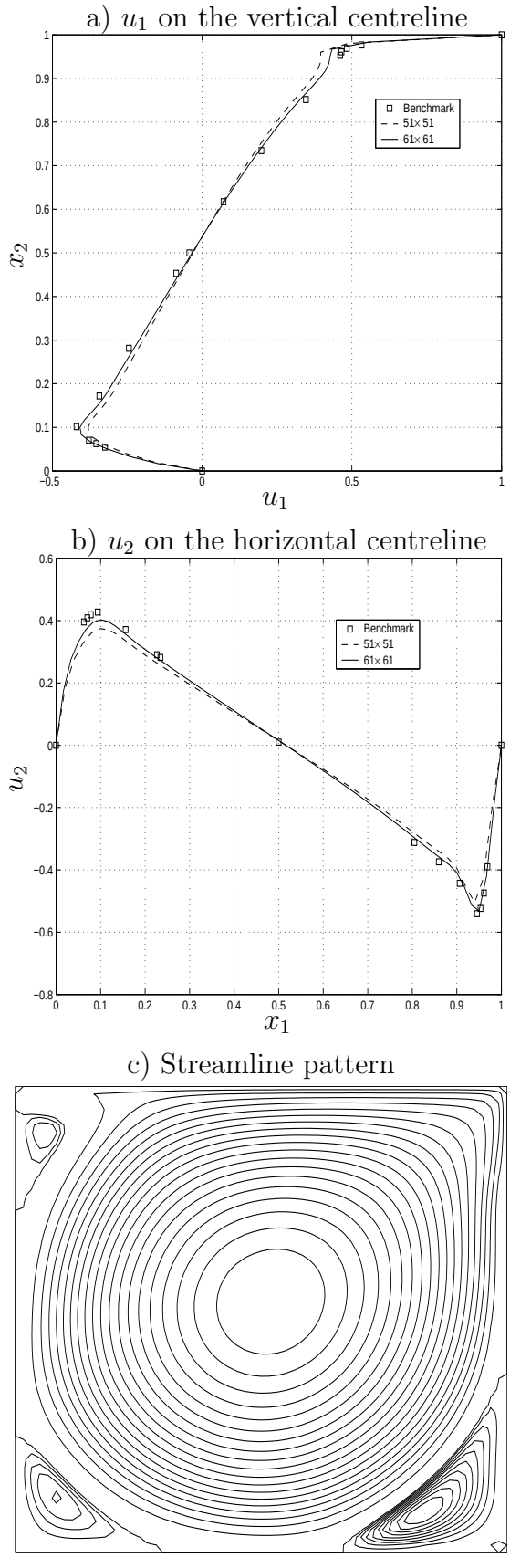

Figure 6: Driven cavity flow, $Re = 3200$: Comparison of velocity profiles along the vertical and horizontal centrelines of the IRBFN method with the benchmark solution (Ghia et al [23] used 129×129 FD mesh). Higher densities of data points yield better accuracy. The streamline pattern obtained with a density of 61×61 is also displayed, where secondary vortices are clearly captured.